Chemical Science

ROYAL SOCIETY OF CHEMISTRY

EDGE ARTICLE

View Article Online
View Journal

Cite this: DOI: 10.1039/d6sc00607h

All publication charges for this article have been paid for by the Royal Society of Chemistry

Ultrafast and high-precision 3D printing *via* type-I-initiated xanthate-mediated RAFT polymerization

Zhihan Yuan, Yixiang Zhang, Ying Meng, Xiaofeng Pan, Na Li,* Jiajia Li* and Jian Zhu*

Received 22nd January 2026
Accepted 26th May 2026

DOI: 10.1039/d6sc00607h

rsc.li/chemical-science

Photopolymerization-based 3D printing offers outstanding spatial and temporal control; however, achieving high build speeds without sacrificing network precision remains challenging, particularly for living/controlled polymerization systems. Herein, we report an ultrafast, high-resolution photo-RAFT 3D printing platform enabled by xanthates in combination with a Norrish type I photoinitiator. This strategy allows practical build speeds (3–30 cm h^{-1}) even at high RAFT concentrations. Through rational modification of the xanthate Z group and blending of xanthates with distinct controllability, the homogeneity and mechanical properties of the polymer networks can be continuously tuned without compromising printing fidelity. The printed objects retain active RAFT chain ends, enabling post-printing welding and multimaterial integration. This work establishes a versatile, application-oriented RAFT-based 3D printing framework that integrates ultrafast fabrication, precise network control, and programmable mechanical functionality.

Introduction

Three-dimensional (3D) printing, or additive manufacturing, has rapidly emerged as a transformative technology across aerospace, microelectronics, biomedical engineering, and soft robotics, enabling rapid prototyping and the fabrication of complex, customized objects directly from digital models.[1–5] Among the various manufacturing routes, photopolymerization-based 3D printing has become the dominant strategy for constructing tailored polymeric materials owing to its high spatial resolution and precise temporal control.[6–11] Although substantial efforts have been devoted to optimizing resin formulations to tailor material properties, comparatively less attention has been paid to regulating the polymerization process itself—despite its critical role in determining polymer network structure and, consequently, the ultimate performance of printed materials. Conventional photopolymerization-based 3D printing predominantly relies on free-radical, cationic, or hybrid polymerization mechanisms, which inherently provide limited control over polymer network formation. In contrast, living/controlled polymerization techniques, such as living cationic polymerization and reversible deactivation radical polymerization (RDRP), offer exceptional control over molecular weight, molecular weight distribution, monomer sequence, and polymer topology.[12–14] Beyond molecular-level precision, these techniques also enable controlled network formation, thereby holding considerable promise for photopolymerization-based 3D printing.[15–20] However, their practical implementation in photoinduced 3D printing remains challenging due to intrinsic limitations, including slow polymerization rates, the frequent requirement for inert atmospheres, and limited tolerance to ambient conditions.

A major breakthrough was achieved in 2019, when reversible addition–fragmentation chain-transfer (RAFT) polymerization—one of the most versatile RDRP methods—was successfully adapted for photoinduced 3D printing. Boyer and coworkers developed photoinduced electron/energy transfer-RAFT (PET-RAFT) 3D printing, which operates under open-air conditions and affords a build speed of 1.2 cm h^{-1}, enabling excellent control over the mechanical properties of printed objects and allowing post-printing functionalization.[21] Jin and Bagheri subsequently demonstrated photoiniferter RAFT 3D printing, which requires neither external photoinitiators nor photocatalysts; however, deoxygenation is necessary and the attainable build speed is limited (<0.5 cm h^{-1}).[22] Later, Norrish type I photoinitiated RAFT (NTI-RAFT) polymerization was introduced, enabling rapid, high-resolution 3D printing with build speeds increased to 9.1 cm h^{-1}.[23] Our group further reported oxygen-tolerant and accelerated 3D printing *via* xanthate-mediated photoiniferter RAFT polymerization, achieving faster build speeds than those obtained using trithiocarbonates.[24] More recently, Wu, Boyer, and An developed an open-air, ultrafast photoiniferter polymerization system for

State Local Joint Engineering Laboratory for Novel Functional Polymeric Materials, Jiangsu Key Laboratory of Advanced Functional Polymer Design and Application, Suzhou Key Laboratory of Macromolecular Design and Precision Synthesis, Department of Polymer Science and Engineering, College of Chemistry Chemical Engineering and Materials Science, Soochow University, Suzhou 215123, China. E-mail: chemlina@suda.edu.cn; chemjjli@suda.edu.cn; chemzhujian@suda.edu.cn

3D printing of low-viscosity resins using a computer-guided molecularly designed photoiniferter (8 s per layer).[25] Other RDRP techniques have also been elegantly incorporated into photoinduced 3D printing. Spangenberg and co-workers realized two-photon-induced nitroxide-mediated polymerization (NMP) for 3D direct laser writing, enabling multimaterial microstructures through successive photoinduced surface reconfigurations.[26] Pang and colleagues developed a visible-light-induced ATRP system employing carbon quantum dots (CQDs) as photocatalysts, enabling ATRP-based 3D printing of hydrogels under aqueous conditions.[27] In addition, our group demonstrated that cationic RAFT polymerization offers significant advantages for 3D printing, including faster polymerization kinetics and diminished retardation effects, allowing higher RAFT concentrations to be employed and thereby expanding the mechanical tunability of printed networks.[28–30]

Despite these advances, further enhancing RAFT-based 3D printing speed, particularly at high RAFT concentrations remains challenging, which is essential for tuning the mechanical properties of the printed materials. Although NTI-RAFT can achieve high build speeds, these were obtained using large layer thicknesses, which compromise *z*-axis resolution.[23] Moreover, the relatively low RAFT concentrations limit the tunable range of mechanical properties. Herein, we report an ultrafast, high-precision RAFT-based 3D printing strategy that employs xanthates in combination with a Norrish type I photoinitiator, enabling rapid printing even at high RAFT agent concentrations. By modifying the Z group of the xanthate chain transfer agent (CTA), we retain excellent control over network formation while significantly accelerating the polymerization rate. Furthermore, blending xanthates with different controllability enables precise modulation of the mechanical properties of the printed networks. The versatility and performance of this platform establish a robust and application-oriented RAFT-based 3D printing methodology that integrates rapid polymerization, high structural fidelity, and tunable material functionality.

Results and discussion

To construct a fast RAFT-3D printing platform, we first evaluated the polymerization kinetics of a model resin composed of poly(ethylene glycol) diacrylate ($PEGDA_{200}$), a xanthate (ethyl 2-((ethoxycarbonothioyl)thio)propanoate, EXEP), and a Norrish type I photoinitiator (diphenyl(2,4,6-trimethylbenzoyl) phosphine oxide, TPO) (Fig. 1A). Real-time attenuated total reflection Fourier-transform infrared (ATR-FTIR) spectroscopy revealed that polymerization proceeded sluggishly and more than 30 s was required to achieve high monomer conversion in the absence of TPO (Fig. 1B). By contrast, the formulations containing TPO reached a conversion plateau within 10 s, indicating that TPO markedly accelerates the consumption of the dissolved oxygen (Fig. 1C). A ratio of $[CTA]_0 : [TPO]_0 = 1 : 0.15$ was adopted for subsequent experiments due to that excess initiator may compromise polymer chain-end fidelity. Increasing the EXEP loading up to 20 mol% relative to PEGDA did not diminish the rapid polymerization kinetics (plateau within 15 s; Fig. 1D), highlighting the robustness of the EXEP/TPO system even at high RAFT concentrations. For comparison, a trithiocarbonate, 2-ethylthiocarbonylsulfanyl-propionic acid ethyl ester (ETSPE), in which the Z-group oxygen of EXEP is replaced with sulfur, was utilized for the photopolymerization. Under identical conditions, ETSPE exhibited significant monomer conversion only at low CTA loadings and low conversion even after 60 s at higher loadings (Fig. 1E). This behaviour can be attributed to pronounced retardation and the light absorption of the RAFT agent, which interferes with the photoinitiator, thereby evidencing less favourable kinetics for high-speed printing.

The practical printing performance of these resins was evaluated using a commercial digital light processing (DLP) 3D printer (M-One Pro, 405 nm, 6 mW cm^{-2}). The actual build speeds (v) were calculated based on target layer thickness, exposure time per layer, target and actual sample thickness and calculated using the following equation:

$$v = \frac{l_1 l_2}{t l_3}$$

where t represents exposure time per layer and l_1, l_2 and l_3 are target layer thickness, actual sample thickness and target sample thickness, respectively. As summarized in Fig. 2A and Table S1, v increased as the TPO loading was raised from 0.10 to 0.15 equiv. relative to the CTA, whereas further increases in TPO had a negligible effect, indicating saturation of the radical flux. Under the optimized conditions (0.15 equiv. TPO and

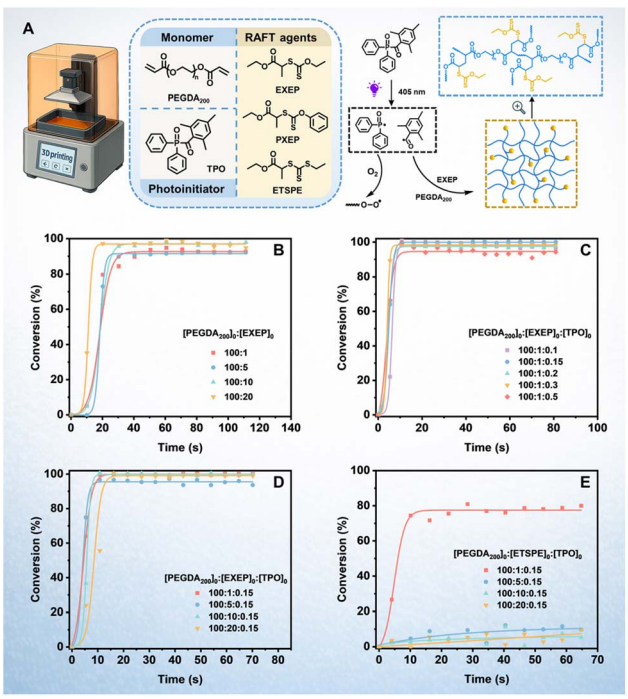

Fig. 1 (A) Resin formulations used for the RAFT-3D printing. Monomer conversion *versus* time with different resin formulations: (B) $[PEGDA_{200}]_0 : [EXEP]_0 = 100 : x$; (C) $[PEGDA_{200}]_0 : [EXEP]_0 : [TPO]_0 = 100 : 1 : x$; (D) $[PEGDA_{200}]_0 : [EXEP]_0 : [TPO]_0 = 100 : x : 0.15$; (E) $[PEGDA_{200}]_0 : [ETSPE]_0 : [TPO]_0 = 100 : x : 0.15$.

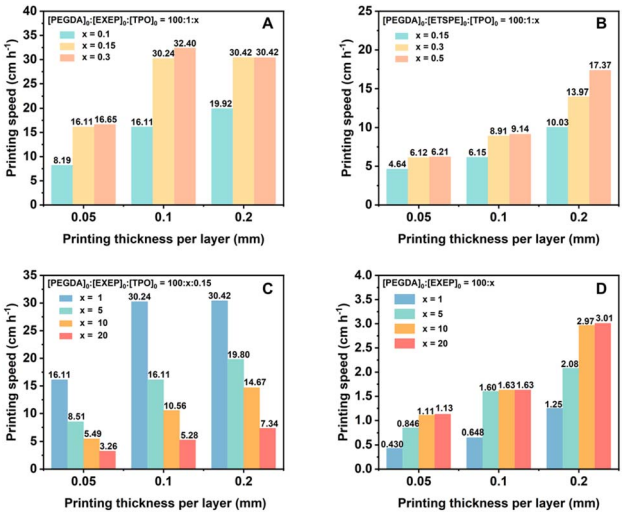

Fig. 2 Printing speed of different printing thickness per layer with a molar ratio of (A) $[PEGDA_{200}]_0 : [EXEP]_0 : [TPO]_0 = 100 : 1 : x$; (B) $[PEGDA_{200}]_0 : [ETSPE]_0 : [TPO]_0 = 100 : 1 : x$; (C) $[PEGDA_{200}]_0 : [EXEP]_0 : [TPO]_0 = 100 : x : 0.15$; (D) $[PEGDA_{200}]_0 : [EXEP]_0 = 100 : x$.

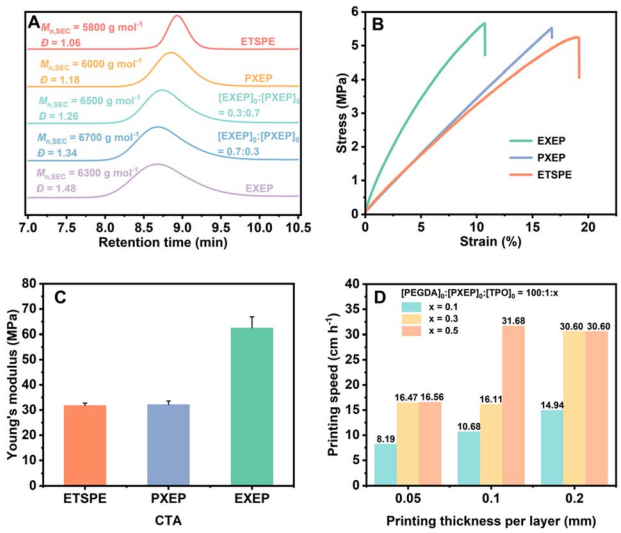

Fig. 3 (A) SEC curves of PBA obtained in Table 1; (B) stress–strain curve and (C) Young's modulus of dumbbell-shaped specimens printed using different CTAs with a molar ratio of $[PEGDA_{200}]_0 : [CTA]_0 : [TPO]_0 = 100 : 1 : 0.3$; (D) build speeds of PXEP-formulated resins with a molar ratio of $[PEGDA_{200}]_0 : [PXEP]_0 : [TPO]_0 = 100 : 1 : x$ with different printing thickness per layer.

a 0.10 mm layer thickness), build speeds exceeding 30 cm h^{-1} were consistently achieved with an exposure time of only 1 s per layer—the hardware minimum—suggesting that even higher speeds may be attainable with faster light modulation. In contrast, ETSPE-based resin formulations exhibited substantially lower build speeds (4.6–10.0 cm h^{-1} over printing thickness per layer of 0.05–0.20 mm; Fig. 2B and Table S2), even when the TPO content was increased to 50 mol% of the CTA. At higher ETSPE loadings, printing failure and poor cure fidelity were observed, restricting their practical utility. Conversely, EXEP-based systems tolerated CTA loadings as high as 20 mol% relative to PEGDA while maintaining acceptable ν values (Fig. 2C and Table S3), thereby providing a broader compositional window for tuning the mechanical properties of the printed objects. For comparison, build speeds were also measured for photoiniferter RAFT systems operating without a type I photoinitiator. As shown in Fig. 2D and Table S4, the maximum attainable build speed under these conditions was limited to 3.01 cm h^{-1}. Notably, this value was achieved only at high EXEP concentrations, likely because initiating radicals are generated through direct photolysis of the xanthate. The build speed of a formulation lacking EXEP was also evaluated and found to be comparable to that of the EXEP/TPO system (Table S5), indicating that incorporation of an appropriate amount of EXEP does not adversely affect printing speed. These results underscore the practical viability and robustness of the proposed RAFT-based 3D printing platform.

Although EXEP exhibits a significantly accelerated polymerization rate, its relatively modest control over the polymerization process leads to broader molecular weight distributions and stiffer polymer networks compared to trithiocarbonates. To address this limitation, we explored another xanthate, ethyl 2-

Table 1 RAFT polymerization of BA with a molar ratio of $[BA]_0 : [CTA]_0 = 50 : 1$ under 405 nm LED light irradiation (60 mW cm^{-2}) at 25 °C

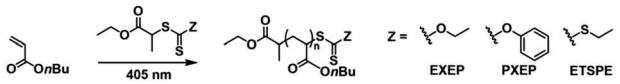

Entry	CTA	Time (min)	Conv. (%)	$M_{n,th}$ [a]	$M_{n,SEC}$ [b]	$Đ$
1	EXEP	5	98.3	6500	6300	1.48
2	PXEP	7	97.2	6500	6000	1.18
3	ETSPE	480	93.4	6200	5800	1.06
4	$[EXEP]_0 : [PXEP]_0 = 0.7 : 0.3$	5	95.7	6400	6700	1.34
5	$[EXEP]_0 : [PXEP]_0 = 0.3 : 0.7$	5	98.6	6600	6500	1.26

[a] Calculated based on conversion ($M_{n,th} = [M]_0/[CTA]_0 \times M_{BA} \times$ conversion + M_{CTA}). [b] Determined by tetrahydrofuran (THF) SEC using polystyrene (PS) calibration.

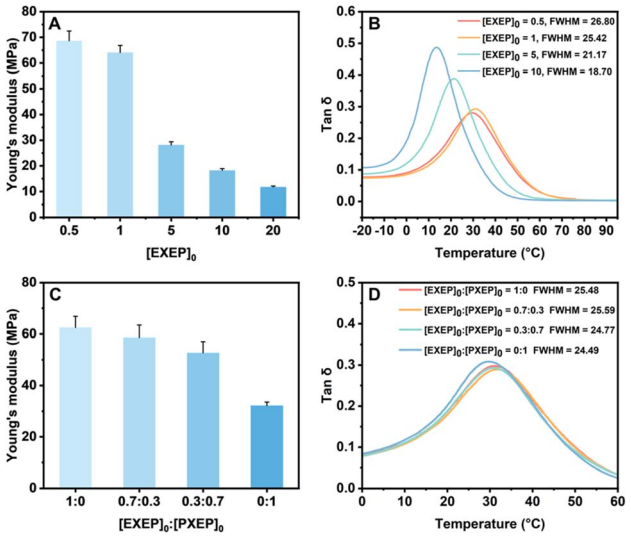

Fig. 4 (A) Young's modulus of dumbbell-shaped specimens printed using EXEP with a molar ratio of $[PEGDA_{200}]_0 : [EXEP]_0 : [TPO]_0 = 100 : x : 0.15$; (B) tan δ *versus* temperature curves of dumbbell-shaped specimens printed using EXEP with a molar ratio of $[PEGDA_{200}]_0 : [EXEP]_0 : [TPO]_0 = 100 : x : 0.15$; (C) Young's modulus of dumbbell-shaped specimens printed using EXEP and PXEP with a molar ratio of $[PEGDA_{200}]_0 : [EXEP]_0 : [PXEP]_0 : [TPO]_0 = 100 : a : b : 0.3$; (D) tan δ *versus* temperature curves of dumbbell-shaped specimens printed using EXEP and PXEP with a molar ratio of $[PEGDA_{200}]_0 : [EXEP]_0 : [PXEP]_0 : [TPO]_0 = 100 : a : b : 0.3$.

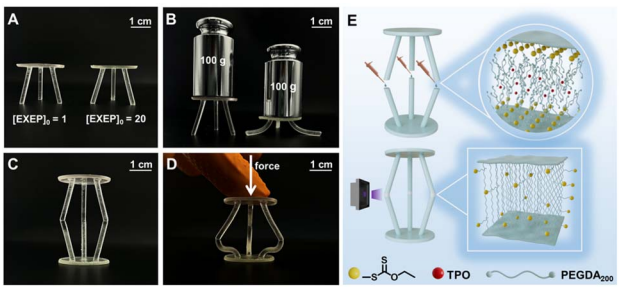

Fig. 5 Digital image of (A) the printed tables with no weights; (B) the printed tables supporting 100 g weights; (C) the welded tables; (D) the welded tables exerted by a downward force; (E) the mechanism of polymer welding.

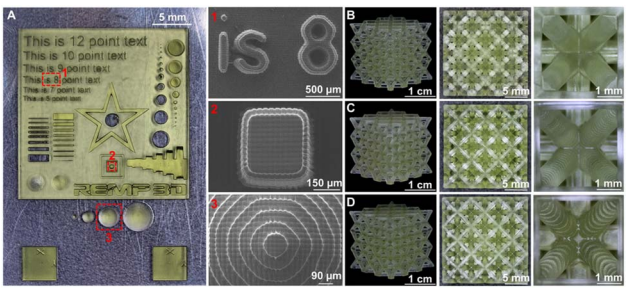

Fig. 6 (A) Digital and SEM images of the printed precision model; digital image of the printed hollow grid model with a printing thickness per layer of (B) 0.05 mm; (C) 0.1 mm; (D) 0.2 mm.

((phenoxycarbonothioyl)thio) propanoate (PXEP), which has demonstrated excellent control in visible light-induced RAFT polymerization.[31] As depicted in Table 1, photoinduced RAFT polymerization of butyl acrylate (BA) using EXEP, PXEP, and ETSPE yielded polymers with dispersities ($Đ$) of 1.48, 1.18, and 1.06, respectively (entries 1–3), indicating that PXEP markedly improves controllability compared to EXEP while retaining a reasonably fast polymerization rate, achieving monomer conversion exceeding 90% within 7 minutes. Importantly, blending EXEP and PXEP at defined molar ratios enables systematic modulation of dispersity, providing a facile strategy for tuning polymer network microstructure and the resulting macroscopic properties. Furthermore, the successful chain extension of all these polymers suggested high chain-end fidelity (Fig. S1).

Tensile testing of dumbbell-shaped specimens printed using different CTAs under optimized conditions ($[PEGDA_{200}]_0 : [CTA]_0 : [TPO]_0 = 100 : 1 : 0.3$) was performed to evaluate their influence on mechanical performance. Moreover, all printed objects were post-cured in a photocuring oven for 10 minutes to further consume the residual monomer. As shown in Fig. 3B and C, materials derived from PXEP and ETSPE exhibited comparable Young's moduli, whereas EXEP-based networks displayed significantly higher stiffness, indicative of a more heterogeneous network architecture arising from reduced control over polymer chain growth. Crucially, PXEP-formulated resins achieved build speeds comparable to those of EXEP systems (Fig. 3D and Table S6), thereby establishing PXEP as a superior CTA for balancing polymerization rate and network controllability in RAFT-based 3D printing.

Furthermore, the mechanical properties of the printed materials can be continuously tuned by varying the CTA composition.[32,33] Increasing EXEP content from 0.5 to 20 mol% systematically reduced Young's modulus (Fig. 4A). Meanwhile, dynamic mechanical analysis (DMA) revealed that the full width at half maximum (FWHM) of the tan δ peaks decreased with increasing CTA concentration (Fig. 4B), indicating the formation of a more homogeneous network with reduced chain entanglement, which is consistent with the tensile test results. In addition, blending EXEP and PXEP enabled precise modulation of network stiffness by adjusting their molar ratios (Fig. 4C). A higher PXEP content resulted in a lower Young's modulus and narrower FWHM (Fig. 4D), verifying that PXEP provides better controllability than EXEP over network formation.

These macroscopic trends demonstrate the effective modulation of printed network properties afforded by RAFT polymerization. The practical impact of these tunable materials was further verified by printing two macroscale objects using formulations that differed only in EXEP content. Under an applied load of 100 g, the high-EXEP (20 mol% of $PEGDA_{200}$) object exhibited substantially greater deformation than its low-EXEP (1 mol% of $PEGDA_{200}$) counterpart (Fig. 5A and B). Moreover, objects with distinct mechanical properties could be welded after surface coating with PEGDA and TPO followed by light irradiation, owing to the preservation of RAFT chain ends, which enables post-printing modification. The interfaced

components fused robustly and displayed differential deformation under external force, illustrating a versatile strategy for the construction of multimaterial architectures (Fig. 5C–E).

To evaluate the printing resolution, a precision model was fabricated using a formulation composed of $[PEGDA_{200}]_0 : [EXEP]_0 : [TPO]_0 = 100 : 1 : 0.3$. As shown in Fig. S4, scanning electron microscopy revealed sharply defined features and smooth surfaces at 50 μm resolution, although slight overcuring was observed at the edges of the printed model. The addition of a small amount of curcumin (0.28 mol% of CTA) as a UV blocker further enhanced the printing resolution (Fig. 6A). Furthermore, hollow grid models were printed at layer thicknesses of 200, 100, and 50 μm, respectively, with exposure times of 2 s, 2 s, and 1 s per layer. All constructs exhibited well-resolved geometries and high build speeds (Fig. 6B–D), demonstrating that rapid printing and fine structural resolution can be simultaneously achieved in this photo-RAFT system.

Conclusions

In summary, we have developed an ultrafast, high-precision photoinduced RAFT-3D printing strategy by integrating xanthate-mediated polymerization with type I photoinitiation. This approach overcomes limitations of RAFT-3D printing, namely slow polymerization rates and restricted RAFT loading, by enabling rapid build speeds (>30 cm h^{-1}) while maintaining excellent network control and high printing resolution. Through rational xanthate design and blending, polymerization kinetics and network homogeneity can be systematically modulated, allowing predictable tuning of mechanical properties. Importantly, the preservation of RAFT chain ends permits post-printing welding and multimaterial assembly, extending the functionality of printed objects beyond static structures. Collectively, this work establishes a robust and generalizable RAFT-3D printing platform that bridges high-throughput manufacturing with precision polymer network engineering.

Author contributions

Zhihan Yuan: writing – original draft, data curation, investigation; Yixiang Zhang: investigation, data curation; Ying Meng: investigation; Xiaofeng Pan: investigation, data curation; Na Li: supervision, writing – review & editing; Jiajia Li: conceptualization, supervision, writing – review & editing, funding acquisition; Jian Zhu: conceptualization, supervision, funding acquisition, writing – review & editing, project administration.

Conflicts of interest

There are no conflicts to declare.

Data availability

The data supporting this article have been included as part of the supplementary information (SI). Supplementary information: materials, instrumentation, detailed experimental procedures, supplementary figures (Fig. S1–S10) and supplementary tables (Tables S1–S8). See DOI: https://doi.org/10.1039/d6sc00607h.

Acknowledgements

This work was supported by the National Natural Science Foundation of China (No. 22371199 and 22571219), the Youth Science and Technology Talent Support Program of Jiangsu Province (JSTJ-2025-391), Basic Science (Natural Science) Research Project of Higher Education Institutions in Jiangsu Province (25KJB150030), the Suzhou Cutting-edge Technology Research Project (SYG202350), the Priority Academic Program Development (PAPD) of Jiangsu Higher Education Institutions, the Program of Innovative Research Team of Soochow University and the Undergraduate Training Program for Innovation and Entrepreneurship, Soochow University (No. 202410285191Y), Postgraduate Research & Practice Innovation Program of Jiangsu Province (KYCX25_3442).

Notes and references

1 C. Yu, J. Schimelman, P. Wang, K. L. Miller, X. Ma, S. You, J. Guan, B. Sun, W. Zhu and S. Chen, *Chem. Rev.*, 2020, **120**, 10695–10743.
2 B. Narupai and A. Nelson, *ACS Macro Lett.*, 2020, **9**, 627–638.
3 J. Mauriello, R. Maury, Y. Guillaneuf and D. Gigmes, *Adv. Mater. Technol.*, 2023, **8**, 2300366.
4 Y. Wang, H. Cui, T. Esworthy, D. Mei, Y. Wang and L. G. Zhang, *Adv. Mater.*, 2022, **34**, 2109198.
5 M. R. Hartings and Z. Ahmed, *Nat. Rev. Chem.*, 2019, **3**, 305–314.
6 S. C. Gauci, A. Vranic, E. Blasco, S. Bräse, M. Wegener and C. Barner-Kowollik, *Adv. Mater.*, 2024, **36**, 2306468.
7 A. Bagheri and J. Jin, *ACS Appl. Polym. Mater.*, 2019, **1**, 593–611.
8 Y. Zhang, Y. Xu, A. Simon-Masseron and J. Lalevée, *Chem. Soc. Rev.*, 2021, **50**, 3824–3841.
9 K. Ehrmann and C. Barner-Kowollik, *J. Am. Chem. Soc.*, 2023, **145**, 24438–24446.
10 T. O. Machado, C. J. Stubbs, V. Chiaradia, M. A. Alraddadi, A. Brandolese, J. C. Worch and A. P. Dove, *Nature*, 2024, **629**, 1069–1074.
11 B. Yang, T. Ni, J. Wu, Z. Fang, K. Yang, B. He, X. Pu, G. Chen, C. Ni, D. Chen, Q. Zhao, W. Li, S. Li, H. Li, N. Zheng and T. Xie, *Science*, 2025, **388**, 170–175.
12 V. A. Bobrin, J. Zhang, N. Corrigan and C. Boyer, *Adv. Mater. Technol.*, 2023, **8**, 2201054.
13 A. Bagheri, C. M. Fellows and C. Boyer, *Adv. Sci.*, 2021, **8**, 2003701.
14 A. Bagheri, *Macromolecules*, 2023, **56**, 1778–1797.
15 G. Moad, *Polym. Int.*, 2015, **64**, 15–24.
16 S. V. Wanasinghe, M. Sun, K. Yehl, J. Cuthbert, K. Matyjaszewski and D. Konkolewicz, *ACS Macro Lett.*, 2022, **11**, 1156–1161.
17 J. Cuthbert, S. V. Wanasinghe, K. Matyjaszewski and D. Konkolewicz, *Macromolecules*, 2021, **54**, 8331–8340.

18 I. O. Raji, O. J. Dodo, N. K. Saha, M. Eisenhart, K. M. Miller, R. Whitfield, A. Anastasaki and D. Konkolewicz, *Angew. Chem., Int. Ed.*, 2024, **63**, e202315200.
19 E. Goldbach, X. Allonas, C. Croutxé-Barghorn, C. Ley, L. Halbardier and G. L'Hostis, *Eur. Polym. J.*, 2023, **188**, 111947.
20 Z. Zhang, N. Corrigan and C. Boyer, *Macromolecules*, 2021, **54**, 1170–1182.
21 Z. Zhang, N. Corrigan, A. Bagheri, J. Jin and C. Boyer, *Angew. Chem., Int. Ed.*, 2019, **58**, 17954.
22 A. Bagheri, K. E. Engel, C. W. A. Bainbridge, J. Xu, C. Boyer and J. Jin, *Polym. Chem.*, 2020, **11**, 641–647.
23 K. Lee, N. Corrigan and C. Boyer, *Angew. Chem., Int. Ed.*, 2021, **60**, 8839.
24 B. Zhao, J. Li, Y. Xiu, X. Pan, Z. Zhang and J. Zhu, *Macromolecules*, 2022, **55**, 1620–1628.
25 Z. Zhang, D. Su, M. Zhang, Z. An, C. Boyer and C. Wu, *Angew. Chem., Int. Ed.*, 2025, e19602.
26 M. Belqat, X. Wu, J. Morris, K. Mougin, T. Petithory, L. Pieuchot, Y. Guillaneuf, D. Gigmes, J.-L. Clément and A. Spangenberg, *Adv. Funct. Mater.*, 2023, **33**, 2211971.
27 L. Qiao, M. Zhou, G. Shi, Z. Cui, X. Zhang, P. Fu, M. Liu, X. Qiao, Y. He and X. Pang, *J. Am. Chem. Soc.*, 2022, **144**, 9817–9826.
28 B. Zhao, J. Li, X. Pan, Z. Zhang, G. Jin and J. Zhu, *ACS Macro Lett.*, 2021, **10**, 1315–1320.
29 B. Zhao, J. Li, G. Li, X. Yang, S. Lu, X. Pan and J. Zhu, *Small*, 2023, **19**, 2207637.
30 B. Zhao, J. Li, C. Yang, X. Pan, Z. Zhang and J. Zhu, *Sci. China: Chem.*, 2025, **68**, 2010–2016.
31 J. Li, C. Ding, Z. Zhang, X. Pan, N. Li, J. Zhu and X. Zhu, *Macromol. Rapid Commun.*, 2017, **38**, 1600482.
32 Z. Yuan, G. Li, C. Yang, W. Zhu, J. Li and J. Zhu, *Chem.–Asian J.*, 2024, **19**, e202400648.
33 G. Li, B. Zhao, Y. Zhu, S. He, J. Li, J. Zhu and N. Li, *Macromol. Rapid Commun.*, 2024, **45**, 2400515.